Analysis of deterministic swapping of photonic and atomic states through single-photon Raman interaction

Serge Rosenblum, Adrien Borne, and Barak Dayan*
Department of Chemical Physics, Weizmann Institute of Science, Rehovot 76100, Israel
(Received 12 December 2016; published 16 March 2017)

The long-standing goal of deterministic quantum interactions between single photons and single atoms was recently realized in various experiments. Among these, an appealing demonstration relied on single-photon Raman interaction (SPRINT) in a three-level atom coupled to a single-mode waveguide. In essence, the interference-based process of SPRINT deterministically swaps the qubits encoded in a single photon and a single atom, without the need for additional control pulses. It can also be harnessed to construct passive entangling quantum gates, and can therefore form the basis for scalable quantum networks in which communication between the nodes is carried out only by single-photon pulses. Here we present an analytical and numerical study of SPRINT, characterizing its limitations and defining parameters for its optimal operation. Specifically, we study the effect of losses, imperfect polarization, and the presence of multiple excited states. In all cases we discuss strategies for restoring the operation of SPRINT.

DOI: 10.1103/PhysRevA.95.033814

I. INTRODUCTION

Optical photons are widely considered prime candidates for the transmission of quantum information from one material quantum node, responsible for processing and storage, to another [1]. Such photonic links can drastically increase scalability, even with realistic error rates [2,3]. A prerequisite for a hybrid quantum system is a reliable interface between its photonic and material qubits. Such an interface also has the prospect of creating an effective interaction between different photons, and may therefore act as a platform for all-optical quantum information processing. Recently, much experimental progress has been made towards this goal, mostly in the field of cavity quantum electrodynamics (cavity QED) [4,5]. In particular, the powerful scheme proposed by Duan and Kimble [6], in which microwave or Raman laser beams are used to create a single-atom interferometer that responds to the presence of one photon in the cavity mode, has been used to experimentally realize nondestructive detection of optical photons [7], a phase gate [8], a quantum gate between photons and a single atom [9], a quantum memory [10], and a photon-photon controlled-NOT quantum gate [11].

In this work we focus on a different scheme that is based on single-photon Raman interaction (SPRINT), which occurs in a three-level Λ system coupled to a single-mode waveguide. Originally proposed by Pinotsi and Imamoglu as a deterministic absorber of a single photon [12] and a quantum memory [12,13], the mechanism of SPRINT was shown by Koshino *et al.* to also be able to implement a $\sqrt{\text{SWAP}}$ quantum gate [14–16] that forms a universal set of quantum gates together with single-qubit operations. Later theoretical studies focused on the harnessing of this scheme for photon-photon interactions, such as photon routing and single-photon extraction [17], single-photon addition [18], and single-photon frequency conversion [19,20]. SPRINT was recently demonstrated experimentally, realizing a single-photon router [21] and a single-photon extractor [22] using a single ^{87}Rb atom. Not limited to atomic systems, it was also demonstrated with superconducting qubits for frequency conversion [23] and detection of single microwave photons [24].

The underlying mechanism of SPRINT is illustrated by first considering the simpler case of a lossless two-level system coupled to a single-mode waveguide [Fig. 1(a)]. Assuming the two-level system has no preferential direction, its steady-state response to a weak resonant probe would be to radiate equally to both directions at amplitude x (taking the amplitude of the probe arbitrarily to be 1). In the forward direction, the atomic radiation interferes with the transmitted input, and as a result $t = 1 + x$. In the backward direction there is no such interference, and so $r = x$. Conservation of energy dictates that in steady state $|r|^2 + |t|^2 = 1$. The only nontrivial solution is therefore $x = -1$. Namely, in the weak field limit in which the two-level transition is not saturated, a two-level system reflects all incoming light due to destructive interference between its forward radiation and the probe. This is in fact the very mechanism responsible for the complete reflection from a metallic mirror: The induced displacement of the free charges lags by a $\pi/2$ phase compared to the driving field, and the far-field radiated by the charges lags by another $\pi/2$, leading to destructive interference in the forward direction, and hence to complete reflection [25].

SPRINT relies on a three-level version of this scenario, in which each "leg" of the Λ system (with ground states G_1 and G_2 and excited state e) is coupled to a different mode, for example, a different direction of the waveguide as depicted in Fig. 1(b). The fact that each leg of the Λ system couples to only one direction (and not to both) makes this configuration equivalent to the two-level scenario. Assuming the radiation amplitudes to both directions are equal, the result therefore remains total destructive interference in the forward direction, and the incoming photon will be reflected. Yet, this can only occur through the $e \rightarrow G_2$ transition, if G_1 is the initial ground state of the Λ system. The result is single-photon Raman interaction (SPRINT), namely the Raman transfer of the Λ system from G_1 to G_2 by the action of a single photon. Since a photon arriving from the opposite direction would not interact with the Λ system, leaving it in G_1, we can see that this Λ

*barak.dayan@weizmann.ac.il

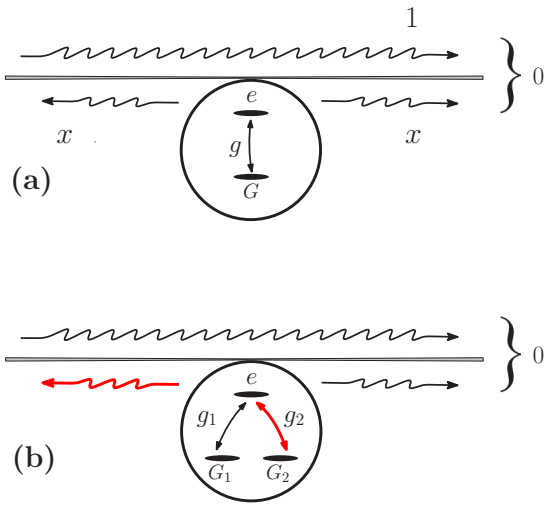

FIG. 1. (a) A two-level system coupled to a single-mode waveguide resulting in complete reflection of the probe. (b) A three-level Λ system in which reflection of a single photon enforces a Raman transfer from one ground state to the other.

system behaves like a passive single-photon memory, in which the direction of the incoming photon is mapped to the resulting state of the Λ system. Additionally, the initial state of the Λ system is mapped to the direction of the outgoing photon. Most importantly, the entire process is coherent and therefore works also for superposition states of both the photon and the Λ system. This means that SPRINT actually performs a quantum SWAP gate between a flying photonic qubit (superposition of modes) and a stationary material qubit (superposition of ground states), and then acts as a quantum memory [13].

In the following section we describe the implementation of SPRINT in Refs. [21,22]. In Sec. III, we analytically model SPRINT, define its fidelity, and analyze various imperfections and the means to minimize their effects. Finally, in Sec. IV we describe the results of a full numerical simulation taking into account most of the practical imperfections present in our experimental realization and discuss the optimal choice of parameters.

II. REALIZATION OF SPRINT WITH A SINGLE ATOM COUPLED TO A WGM RESONATOR

The coupling of material systems to waveguides is typically performed by optical resonators, which provide the necessary Purcell enhancement of the coupling to the guided modes compared to the free-space ones. By confining light inside a very small volume for an extended period of time, the electric field of even a single photon becomes sufficient to significantly affect the dynamics of a quantum emitter (e.g., a single atom) that interacts with the cavity modes.

The most general description of cavity-assisted SPRINT is a Λ system inside a single-sided Fabry-Perot resonator, namely a resonator in which one of the mirrors is a perfect reflector and the other is the input-output coupler (Fig. 2). In the SPRINT configuration, each "leg' of the Λ-system is coupled to a different mode of the resonator—a different frequency, polarization or even spatial mode [17]. In this

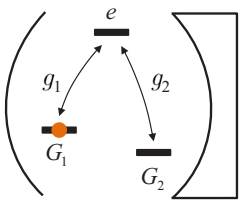

FIG. 2. Schematic of an atomic three-level Λ system inside a single-sided cavity.

work we consider an equivalent configuration based on a whispering-gallery mode (WGM) microresonator [26], in which photons are confined by continuous total internal reflection. The microresonator is nanofiber-coupled, so that photons coming from the left and right in the fiber excite the counterpropagating cavity modes through evanescent-wave coupling (Fig. 3). A single WGM is brought to resonance with a ^{87}Rb atom by tuning the temperature of the microresonator. The other WMGs are assumed to be far-detuned, so that their influence on the dynamics can be neglected.

The equivalence to a single-sided Fabry-Perot cavity is created by using transverse magnetic (TM) modes, which have the remarkable property that their evanescent-wave polarization is circular to a high degree [27–29], with the handedness of the polarization depending on the direction of propagation. This creates the unique situation in which the counterclockwise (a) and clockwise (b) rotating photons may interact with different atomic transitions due to their opposite spin. Specifically, in the case of an atomic Λ system as depicted in the inset of Fig. 3, a interacts only with the σ^+ polarized $G_1 \leftrightarrow e$ transition, whereas b interacts only with the σ^- polarized $G_2 \leftrightarrow e$ transition, thereby creating the necessary single-sided cavity configuration.

III. THEORETICAL MODEL AND INFLUENCE OF LOSSES AND IMPERFECTIONS

The mechanism of SPRINT is most conveniently modeled using quantum trajectory theory with cascaded systems [17,30]. A single-sided source cavity described by its

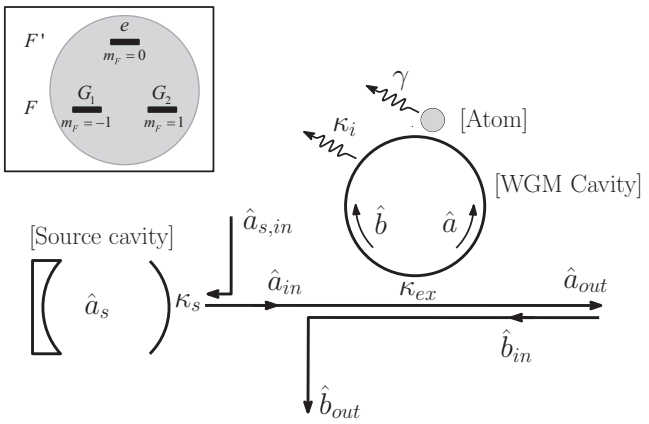

FIG. 3. Schematic of the theoretical model; in inset, the atomic Λ system.

annihilation operator $\hat{a}_s$ and with a decay rate of $2\kappa_s$ emits a single-photon pulse to the right, which then couples to the mode a of the WGM microresonator at a rate $2\kappa_{\rm ex}$. The photon's field then interacts with the atom's left and right ground states (through the excited state) at rates g_1 and g_2, respectively, and eventually leaks back into both directions of the nanofiber, as described by the right and left output field annihilation operators [31]:

$$\hat{a}_{\rm out} = \sqrt{2\kappa_s}\hat{a}_s + \sqrt{2\kappa_{\rm ex}}\hat{a}, \tag{1a}$$

$$\hat{b}_{\rm out} = \sqrt{2\kappa_{\rm ex}}\hat{b}, \tag{1b}$$

where the vacuum input operators $\hat{a}_{s,\rm in}$ and $\hat{b}_{\rm in}$ have been discarded, since we only consider normally ordered operators. Equation (1a) exhibits the fact that a transmitted output photon cannot be exclusively attributed to the event of a photon emitted by the microresonator to the right, or to a transmitted photon that did not enter the microresonator in the first place. Rather, it is the interference between both that creates the resulting output field.

A. Ideal SPRINT model, influence of losses

The Hamiltonian that governs the dynamics of this system is (setting $\hbar = 1$)

$$\begin{aligned}\hat{H}_0 = &-2i\sqrt{\kappa_s\kappa_{ex}}\hat{a}_s\hat{a}^\dagger - i\kappa_s\hat{a}_s^\dagger\hat{a}_s \\ &+ (g_1^*\hat{a}^\dagger\hat{\sigma}_{1e} + g_1\hat{\sigma}_{1e}^\dagger\hat{a}) + (g_2\hat{b}^\dagger\hat{\sigma}_{2e} + g_2^*\hat{\sigma}_{2e}^\dagger\hat{b}) \\ &- i(\kappa + i\delta_C)(\hat{a}^\dagger\hat{a} + \hat{b}^\dagger\hat{b}) - i(\gamma + i\delta_a)\hat{\sigma}_{ee}.\end{aligned} \tag{2}$$

It can be subdivided in three parts. The first row corresponds to the emission from the source cavity into mode a of the microresonator. The driving term is non-unitary, in accordance with the unidirectional character of the interaction. Indeed, the resonator cannot re-emit the photon to the source cavity [30]. The second row describes the Jaynes-Cummings interaction between each of the two counterpropagating WGM modes, and the corresponding atomic transition. Here, $\hat{\sigma}_{ke}$ denotes the lowering operator from the excited state to ground state G_k. The photon-atom coupling rates g_1 and g_2 are complex quantities to account for the motion of the atom during the SPRINT process. Finally, the third row describes detunings and losses of the two WGM modes and the atom. $2\kappa = 2\kappa_{ex} + 2\kappa_i$ is the total WGM decay rate due to coupling to the nanofiber and intrinsic loss, respectively. 2γ is the atomic spontaneous emission rate into free space, which is multiplied by the excited state population σ_{ee}. Among these loss mechanisms, only the coupling to the nanofiber will result in detectable output photons, as emphasized by Eq. (1). The detuning of the atomic transitions δ_a, and the detuning of the cavity modes δ_C with respect to the driving frequency are taken to be zero unless otherwise specified. The two counterpropagating WGMs are degenerate by symmetry, and the two ground states are assumed here to be degenerate as well. However, this degeneracy is not required for SPRINT as long as every mode is resonant with one of the transitions.

The initial state $|\psi(0)\rangle = |1_s0_a0_bG_1\rangle$ containing a photon in the source cavity and an atom prepared in its left ground state evolves according to the Schrödinger equation to

$$\begin{aligned}|\psi(t)\rangle = &\, e^{-\kappa_s t}|1_s0_a0_bG_1\rangle + \alpha(t)|0_s1_a0_bG_1\rangle \\ &+ \beta(t)|0_s0_a1_bG_2\rangle + \xi(t)|0_s0_a0_be\rangle,\end{aligned} \tag{3}$$

with

$$\begin{aligned}\dot{\alpha}(t) &= -2\sqrt{\kappa_s\kappa_{ex}}e^{-\kappa_s t} - ig_1^*\xi - \kappa\alpha, \\ \dot{\beta}(t) &= -ig_2\xi - \kappa\beta, \\ \dot{\xi}(t) &= -ig_1\alpha - ig_2^*\beta - \gamma\xi.\end{aligned} \tag{4}$$

Ideally, long pulses should be used, so that κ_s would become the lowest rate of the system. $|\psi(t)\rangle$ is then close to steady state at all times, and the derivatives can be put equal to zero, yielding

$$\begin{aligned}\alpha(t) &= -2\frac{\sqrt{\kappa_s\kappa_{\rm ex}}}{\kappa}\left[1 - \frac{|g_1|^2}{|g_1|^2+|g_2|^2}\frac{2C_{\rm tot}}{1+2C_{\rm tot}}\right]e^{-\kappa_s t}, \\ \beta(t) &= 2\frac{\sqrt{\kappa_s\kappa_{ex}}}{\kappa}\frac{g_1g_2}{|g_1|^2+|g_2|^2}\frac{2C_{\rm tot}}{1+2C_{\rm tot}}e^{-\kappa_s t}, \\ \xi(t) &= 2i\sqrt{\kappa_s\kappa_{ex}}\frac{g_1}{|g_1|^2+|g_2|^2}\frac{2C_{\rm tot}}{1+2C_{\rm tot}}e^{-\kappa_s t},\end{aligned} \tag{5}$$

where the total cooperativity,

$$C_{\rm tot} = \frac{|g_1|^2+|g_2|^2}{2\kappa\gamma} \tag{6}$$

quantifies the tendency of the atom to emit into both microresonator modes, rather than into free space. In this long-pulse limit, the fact that the source-cavity formalism results in an exponentially decaying input pulse is irrelevant, and the results below apply for any pulse shape. Using Eq. (1) the transmission and reflection probabilities can be calculated, giving

$$T = \int_0^\infty \langle\hat{a}_{\rm out}^\dagger\hat{a}_{\rm out}\rangle\, dt = \left|\frac{2\kappa_{\rm ex}}{\kappa}\frac{|g_1|^2}{|g_1|^2+|g_2|^2}\frac{2C_{\rm tot}}{1+2C_{\rm tot}} + t_0\right|^2, \tag{7a}$$

$$R = \int_0^\infty \langle\hat{b}_{\rm out}^\dagger\hat{b}_{\rm out}\rangle\, dt = \left|\frac{2\kappa_{\rm ex}}{\kappa}\frac{g_1g_2}{|g_1|^2+|g_2|^2}\frac{2C_{\rm tot}}{1+2C_{\rm tot}}\right|^2, \tag{7b}$$

where

$$t_0 = -\frac{\kappa_{\rm ex}-\kappa_i}{\kappa} \tag{8}$$

is the "bare" forward transmission when the atom is absent.

Inspection of Eqs. (7) and (8) reveals three requirements for efficient operation of SPRINT, i.e., for R close to unity: First, the intrinsic loss of the microresonator must be considerably smaller than $\kappa_{\rm ex}$. Secondly, the coupling strengths of the two transitions must be equal in their absolute values [32]. Finally, the cooperativity must be significantly larger than one, ensuring that the spontaneous emission is primarily directed into the mircroresonator, rather than into free space. This situation can be realized both in the strong coupling regime (in which $g \gg \kappa_{\rm ex} \gg \kappa_i, \gamma$) and in the fast-cavity or Purcell regime (with $\kappa_{\rm ex} \gg g \gg \kappa_i, \gamma$).

In a realistic system, photons may be lost to the environment by the resonator or the atom, reducing the efficiency $\eta = R + T$ of the SPRINT process. If the photon is not lost,

various deviations from the ideal model may still cause an undesired final atom-photon state. We will quantify this by defining SPRINT fidelity, the overlap of the final state with the ideal state (reflection of a photon, together with the toggling of the atom) provided the photon was not lost in the process:

$$\mathcal{F} = \frac{P(R,\text{toggle})}{\eta}. \tag{9}$$

Note that the SPRINT fidelity effectively provides the lower bound on the SWAP gate fidelity. This is because the SWAP operation involves the case in which both the photonic and the atomic states are toggled together and the case in which no interaction should occur, the fidelity of the latter being obviously larger than the fidelity of the former. For this reason, we focus in this work on $\mathcal{F}$, the fidelity of the first case.

Equation (7a) shows that for ideal SPRINT operation, the forward radiation of the atom and the forward transmission when the atom is absent should have equal magnitude but opposite sign, leading to perfect destructive interference. This may suggest that limited cooperativity and intrinsic resonator losses will cause nonzero transmission, and hence a reduced SPRINT fidelity. However, SPRINT fidelity can always be unity by choosing

$$\kappa_{\text{ex}}^{\text{opt}} = \kappa_i\sqrt{1+2C_i}, \tag{10}$$

where we took $g_1 = g_2 \equiv g$, and defined the total intrinsic cooperativity $C_i = |g|^2/\kappa_i\gamma$. Hence, by tuning the coupling strength (for example, by varying the distance between the microresonator and the nanofiber), one can ensure that complete destructive interference is maintained in the forward direction. The photon can then either be reflected, or lost due to dissipation, but never transmitted—allowing heralded operation of SPRINT. One can gain more insight by noting that for large enough intrinsic cooperativity Eq. (10) becomes $2\kappa_i/\kappa^2 = \gamma/|g|^2$, suggesting that the loss rate in the cavity should compensate for the loss rate in the atom. Note that in any case κ_i needs to be smaller than κ_{ex}, otherwise the crucial destructive interference becomes a constructive one.

B. Influence of a nonideal circular polarization

This section is dedicated to the study of a nonideal circular polarization in the evanescent part of the WGM. The analytical solution of Maxwell's equations for a microsphere [33] shows the existence of a non-negligible π-polarized (i.e., perpendicular to the WGM plane) electric field, and also a component of circular polarization with opposite handedness. The ratios of the unwanted electric field component to the desired one are denoted r_σ for the opposite circular polarized field, and r_π for the π-polarized field. This nonideal polarization may, for example, cause a photon in mode b to drive a σ^+ transition of the atom, disrupting the SPRINT mechanism.

1. Undesired σ polarization

For the idealized Λ-type three-level system where no π transition is possible, the dynamics with nonideal circular polarization is governed by the following Hamiltonian:

$$\begin{aligned}\hat{H}_1 =& \hat{H}_0 + r_\sigma(g_2^*\hat{a}^\dagger\hat{\sigma}_{2e} + g_2\hat{\sigma}_{2e}^\dagger\hat{a}) + r_\sigma(g_1\hat{b}^\dagger\hat{\sigma}_{1e} + g_1^*\hat{\sigma}_{1e}^\dagger\hat{b})\\ :=& \hat{H}_0 + \hat{H}_{r_\sigma},\end{aligned} \tag{11}$$

with $\hat{H}_0$ the Hamiltonian from Eq. (2). As before, the Schrödinger equation is solved analytically and leads to the transmission and reflection probabilities,

$$\begin{aligned}T =& \left|\frac{2\kappa_{\text{ex}}}{\kappa}\frac{|g_1|^2}{|g_1|^2+|g_2|^2}\frac{2C_{\text{tot}}}{1+2C_{\text{tot}}\left(1+r_\sigma^2\right)} + t_0\right|^2\\ &+\left|r_\sigma\frac{2\kappa_{\text{ex}}}{\kappa}\frac{g_1g_2}{|g_1|^2+|g_2|^2}\frac{2C_{\text{tot}}}{1+2C_{\text{tot}}\left(1+r_\sigma^2\right)}\right|^2\\ :=& T_1 + T_2,\end{aligned} \tag{12a}$$

$$\begin{aligned}R =& \left|r_\sigma\frac{2\kappa_{\text{ex}}}{\kappa}\frac{|g_1|^2}{|g_1|^2+|g_2|^2}\frac{2C_{\text{tot}}}{1+2C_{\text{tot}}\left(1+r_\sigma^2\right)}\right|^2\\ &+\left|\frac{2\kappa_{\text{ex}}}{\kappa}\frac{g_1g_2}{|g_1|^2+|g_2|^2}\frac{2C_{\text{tot}}}{1+2C_{\text{tot}}\left(1+r_\sigma^2\right)}\right|^2\\ :=& R_1 + R_2,\end{aligned} \tag{12b}$$

where t_0 is still given by Eq. (8).

Comparing Eq. (12) with Eq. (7), we see that one additional contribution to both the transmission and reflection probabilities arises from the consideration of a nonzero r_σ: The photonic mode a can now also interact with the σ^- polarized transition $|e\rangle \to |G_2\rangle$ (term T_2); and mode b with the σ^+ polarized transition $|e\rangle \to |G_1\rangle$ (term R_1). Note that the SPRINT mechanism (term R_1) dominates for small r_σ since the ratio R_1/R_2 scales as r_σ^2.

From Eq. (9), the fidelity here equals $R_2/(R+T)$. Its optimum, which is no longer unity, can be achieved by choosing the extrinsic coupling rate as

$$\kappa_{\text{ex}}^{\text{opt}} = \kappa_i \times \left(-C_i r_\sigma^2 + \sqrt{1+2C_i\left(1+r_\sigma^2\right)+C_i^2r_\sigma^4}\right), \tag{13}$$

and equals

$$\mathcal{F}\left(\kappa_{\text{ex}}^{\text{opt}}\right) = \frac{1}{1+2r_\sigma^2}, \tag{14}$$

where we took $g_1 = g_2$. Numerical evaluations of this result with realistic parameters will be performed in Sec. V.

2. π polarization

We now consider the effect of the π component of polarization while leaving the undesired σ component aside. The ground state G_0 ($m_F = 0$) is added to the three-level Λ system considered so far and g_0 denotes the coupling rate between the levels G_0 and e. The Hamiltonian becomes

$$\begin{aligned}\hat{H}_2 =& \hat{H}_0 + r_\pi(g_0^*\hat{a}^\dagger\hat{\sigma}_{0e} + g_0\hat{\sigma}_{0e}^\dagger\hat{a}) + r_\pi(g_0\hat{b}^\dagger\hat{\sigma}_{0e} + g_0^*\hat{\sigma}_{0e}^\dagger\hat{b})\\ :=& \hat{H}_0 + \hat{H}_{r_\pi},\end{aligned} \tag{15}$$

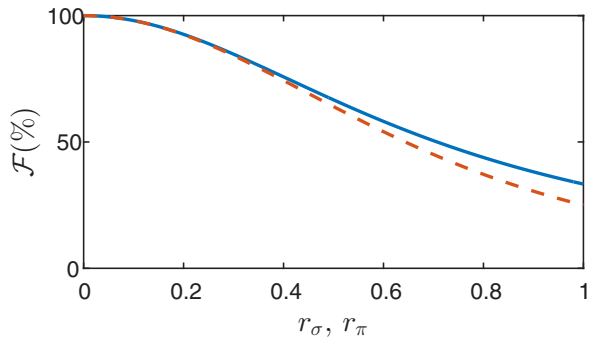

FIG. 4. Fidelity as a function of r_σ or r_π for optimized (solid line) and nonoptimized κ_{ex} (dashed line).

and leads to the transmission and reflection probabilities,

$$T = \left|\frac{2\kappa_{ex}}{\kappa}\frac{|g_1|^2}{|g_1|^2+|g_2|^2}\frac{2C_{tot}}{1+2\left(C_{tot}+2r_\pi^2C_0\right)}+t_0\right|^2 + \left|r_\pi\frac{2\kappa_{ex}}{\kappa}\frac{g_1g_0}{|g_1|^2+|g_2|^2}\frac{2C_{tot}}{1+2\left(C_{tot}+2r_\pi^2C_0\right)}\right|^2 := T_1+T_0, \tag{16a}$$

$$R = \left|\frac{2\kappa_{ex}}{\kappa}\frac{g_1g_2}{|g_1|^2+|g_2|^2}\frac{2C_{tot}}{1+2\left(C_{tot}+2r_\pi^2C_0\right)}\right|^2 + \left|r_\pi\frac{2\kappa_{ex}}{\kappa}\frac{g_1g_0}{|g_1|^2+|g_2|^2}\frac{2C_{tot}}{1+2\left(C_{tot}+2r_\pi^2C_0\right)}\right|^2 := R_2+R_0, \tag{16b}$$

with $C_0=\dfrac{|g_0|^2}{2\kappa\gamma}$.

The choice $g_1=g_2=g_0$ results in a complete analogy between Eqs. (12) and (16) under the exchange of r_σ and r_π. The fidelity is therefore maximized by choosing the extrinsic coupling parameter,

$$\kappa_{ex}^{opt}=\kappa_i\times\left(-C_ir_\pi^2+\sqrt{1+2C_i\left(1+r_\pi^2\right)+C_i^2r_\pi^4}\right), \tag{17}$$

and equals

$$\mathcal{F}\left(\kappa_{ex}^{opt}\right)=\frac{1}{1+2r_\pi^2}. \tag{18}$$

We end this section by comparing the optimal fidelity from Eq. (14) [respectively, Eq. (18)] with the nonoptimized one. The latter can be deduced from Eq. (12) [respectively, Eq. (16)] and, in the case that allows an efficient operation of SPRINT, i.e., $g_1=g_2=g_0$, $\kappa_{ex}\gg\kappa_i$, and $C_t\gg1$, it takes the simple form:

$$\mathcal{F}(\kappa_{ex}\gg\kappa_i)\approx\frac{1}{\left(1+r_j^2\right)^2}, \tag{19}$$

with $j\in\{\sigma,\pi\}$. These quantities are shown in Fig. 4 as a function of r_σ (respectively, r_π), in the optimized (solid line) and nonoptimized (dashed line) cases. For small values of r_σ and r_π, we see that varying κ_{ex} is not beneficial for the fidelity.

C. Influence of the parasitic coupling between optical modes

Rayleigh scattering between the optical modes a and b at a rate $2h$ can also affect the fidelity as a photon can be reflected without the atom being involved. The Hamiltonian including h is given by

$$\hat{H}_3=\hat{H}_0+h(\hat{a}^\dagger\hat{b}+\hat{b}^\dagger\hat{a}):=\hat{H}_0+\hat{H}_h, \tag{20}$$

resulting in the transmission and reflection probability coefficients

$$T = \left|\frac{2\kappa_{ex}}{\kappa+h^2/\kappa}\frac{|g_1|^2}{|g_1|^2+|g_2|^2}\frac{2C_{tot}}{1+h^2/\kappa^2+2C_{tot}}+t_0\right|^2 + \left|r_0\frac{g_1g_2}{|g_1|^2+|g_2|^2}\frac{2C_{tot}}{1+h^2/\kappa^2+2C_{tot}}\right|^2 := T_1+T_2, \tag{21a}$$

$$R = \left|r_0\left(1-\frac{|g_1|^2}{|g_1|^2+|g_2|^2}\frac{2C_{tot}}{1+h^2/\kappa^2+2C_{tot}}\right)\right|^2 + \left|\frac{2\kappa_{ex}}{\kappa+h^2/\kappa}\frac{g_1g_2}{|g_1|^2+|g_2|^2}\frac{2C_{tot}}{1+h^2/\kappa^2+2C_{tot}}\right|^2 := R_1+R_2, \tag{21b}$$

where $t_0=\frac{\kappa_i^2-\kappa_{ex}^2+h^2}{\kappa^2+h^2}$ and $r_0=\frac{2\kappa_{ex}h}{\kappa^2+h^2}$ are, respectively, the transmission and reflection when the atom is absent. Note that the coupling between optical modes results in nonzero r_0.

Comparing Eq. (21) with Eq. (7), we highlight the contributions arising from the optical mode coupling h: a photon emitted in mode $\hat{b}$ through the transition $|e\rangle\to|G_2\rangle$ can be subsequently reflected into $\hat{a}$ (term T_2); and noncomplete destructive interference between the incoming probe and the radiative field can occur in reflection since the mode $\hat{a}$ associated with $|e\rangle\to|G_1\rangle$ can be changed into $\hat{b}$ (term R_1). Note that the event R_1 is rarer than R_2 by a factor $(h/\kappa)^2$, therefore ensuring that reflections can be mostly associated with SPRINT for small values of h.

Then, the value for κ_{ex} resulting in a maximal (although not unit) fidelity is found by numerically solving the equation $\partial_{\kappa_{ex}}\mathcal{F}=0$. When h is small compared to the other system parameters (in particular κ_i), a perturbative resolution of this equation leads to

$$\kappa_{ex}^{opt}=\kappa_i\sqrt{1+2C_i}\times\left[1+\frac{h^2}{\kappa_i^2}\frac{(1+C_i)}{(1+2C_i)(1+\sqrt{1+2C_i})}+o\left(\frac{h^2}{\kappa_i^2}\right)\right], \tag{22}$$

where we again took $g_1=g_2$, and the optimized fidelity equals

$$\mathcal{F}\left(\kappa_{ex}^{opt}\right)=1-\frac{h^2}{\kappa_i^2}\frac{(3+2C_i-2\sqrt{1+2C_i})}{C_i^2}+o\left(\frac{h^2}{\kappa_i^2}\right). \tag{23}$$

D. Influence of r_σ, r_π and h combined

We now consider jointly the nonideal circular polarization and the optical mode coupling in the four-level system $\{G_0,G_1,G_2,e\}$ by deriving its state evolution with the

Hamiltonian:

$$\hat{H}_4 = \hat{H}_0 + \hat{H}_{r_\sigma} + \hat{H}_{r_\pi} + \hat{H}_h. \tag{24}$$

Nonzero h causes the formation of an azimuthally varying field. Since every atomic transition interacts with both a and b due to the nonideal circular polarization, the azimuthal location of the atom, represented by the phase of the coupling constants, starts to play a role.

The transmission and reflection probabilities are given by

$$T = 1 + 2\mathrm{Re}(\alpha_1) + |\alpha_1|^2 + |\alpha_2|^2 + |\alpha_0|^2, \tag{25a}$$

$$R = |\beta_1|^2 + |\beta_2|^2 + |\beta_0|^2, \tag{25b}$$

with

$$\begin{aligned}
\alpha_1 &= -p\left(1 + \frac{u(g_1)u(g_1^*)}{|g_1|^2+|g_2|^2}\frac{2C_{\mathrm{tot}}}{D}\right),\\
\alpha_2 &= p\frac{u(g_1)v(g_2^*)}{|g_1|^2+|g_2|^2}\frac{2C_{\mathrm{tot}}}{D},\\
\alpha_0 &= p\frac{u(g_1)w(g_0)}{|g_1|^2+|g_2|^2}\frac{2C_{\mathrm{tot}}}{D},\\
\beta_1 &= p\left(\frac{h}{\kappa} + \frac{u(g_1)v(g_1)}{|g_1|^2+|g_2|^2}\frac{2C_{\mathrm{tot}}}{D}\right),\\
\beta_2 &= p\frac{u(g_1)u(g_2)}{|g_1|^2+|g_2|^2}\frac{2C_{\mathrm{tot}}}{D},\\
\beta_0 &= p\frac{u(g_1)w(g_0^*)}{|g_1|^2+|g_2|^2}\frac{2C_{\mathrm{tot}}}{D},
\end{aligned} \tag{26}$$

and

$$\begin{aligned}
u(g) &= r_\sigma\frac{h}{\kappa}g^* + ig, \quad v(g) = -r_\sigma g + i\frac{h}{\kappa}g^*,\\
w(g) &= r_\pi\left(\frac{h}{\kappa}g^* + ig\right),\\
D &= 1 + \frac{h^2}{\kappa^2} + 2\left[\left(1+r_\sigma^2\right)C_{\mathrm{tot}} + 2r_\pi^2 C_0\right]\\
&\quad - 4i\frac{h}{\kappa}\left(r_\sigma\tilde{C}_{\mathrm{tot}} + r_\pi^2\tilde{C}_0\right),\\
\tilde{C}_{\mathrm{tot}} &= \frac{\mathrm{Re}\left(g_1^2+g_2^2\right)}{2\kappa\gamma}, \quad \tilde{C}_0 = \frac{\mathrm{Re}\left(g_0^2\right)}{2\kappa\gamma},\\
p &= \frac{2\kappa_{\mathrm{ex}}}{\kappa + h^2/\kappa}.
\end{aligned} \tag{27}$$

The 12 contributions leading to the reflection probabilities $|\beta_1|^2$, $|\beta_2|^2$, and $|\beta_0|^2$ from Eq. (25b) are sketched in Fig. 5, where r_σ represents a transition driven by the unwanted circular polarization, r_π a transition driven by the π polarization, and h stands for the reflection of the photon because of the coupling between optical modes. Among them, the four terms of $|\beta_2|^2$ lead to the desired atomic toggle from G_1 to G_2: The

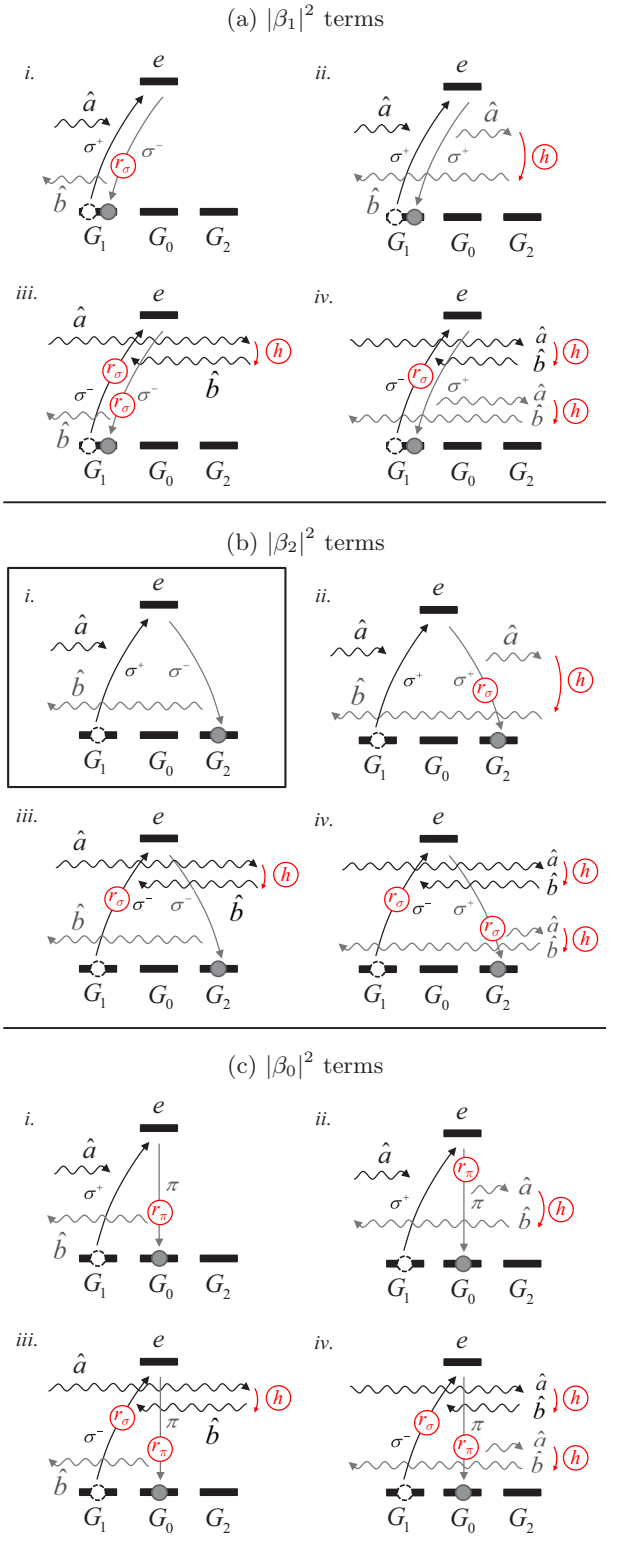

FIG. 5. Illustration of the 12 contributions to the reflection coefficient R, associated with no atomic toggle (a), and an atomic toggle to the state G_2 (b) or to the state G_0 (c). The SPRINT term is shown in a box.

frame i. depicts the actual SPRINT term, and the frames ii. to iv. show the imperfections h and r_σ compensating each other. For small h, r_σ and r_π, this probability $|\beta_2|^2$ exceeds the

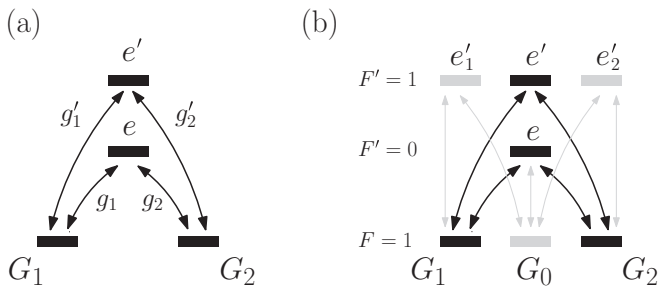

FIG. 6. (a) Two excited states instead of one provide two pathways for SPRINT. Depending on the signs of the coupling strengths, the symmetry required for SPRINT can be either maintained or removed. (b) Actual level scheme of the ^{87}Rb D_2 line. Transitions that are weak due to polarization mismatch are shown in gray. Note that the transition $G_0 \to e'$ is forbidden, and that the effect of the excited state $F' = 2$ is negligible, due to its large detuning and low coupling strength to $F = 1$.

unwanted terms $|\beta_1|^2$ and $|\beta_0|^2$ as follows:

$$\frac{|\beta_1|^2}{|\beta_2|^2} = \frac{h^2}{\kappa^2}\left(\frac{1+C_{\rm tot}}{C_{\rm tot}}\right)^2 + r_\sigma^2 + o\left(\frac{h^i}{\kappa^i} r_\sigma^j\right)_{i+j=2}, \tag{28a}$$

$$\frac{|\beta_0|^2}{|\beta_2|^2} = r_\pi^2 + o\left(\frac{h^i}{\kappa^i} r_\pi^j\right)_{i+j=2}. \tag{28b}$$

E. Multiple excited states

In practical systems, the presence of various excited states [see Fig. 6(a)] can create multiple pathways for Raman passage, which interfere with each other, and therefore affect the operation of SPRINT. The parameters h, r_σ, and r_π being here neglected, this situation can be analyzed by adding to the Hamiltonian of Eq. (2) two Jaynes-Cummings terms corresponding to the second excited state e', along with its associated loss γ' and detuning δ_a':

$$\begin{aligned}\hat{H}_5 &= \hat{H}_0 - i(\gamma' + i\delta_a')\hat{\sigma}_{e'e'} + (g_1'^*\hat{a}^\dagger\hat{\sigma}_{1e'} \\ &\quad + g_1'\hat{\sigma}_{1e'}^\dagger\hat{a}) + (g_2'\hat{b}^\dagger\hat{\sigma}_{2e'} + g_2'^*\hat{\sigma}_{2e'}^\dagger\hat{b}) \\ &:= \hat{H}_0 + \hat{H}_{e'}.\end{aligned} \tag{29}$$

The Schrödinger equations corresponding to this new Hamiltonian can be easily solved by assuming $g_1' = \eta g_1$ and $g_2' = s\eta g_2$, with $s = \pm 1$. In the case of coupling strengths of equal sign, i.e., $s = +1$, we obtain

$$T = \left|\frac{2\kappa_{\rm ex}}{\kappa}\frac{|g_1|^2}{|g_1|^2+|g_2|^2}\frac{2(C_{\rm tot}+C_{\rm tot}')}{1+2(C_{\rm tot}+C_{\rm tot}')} + t_0\right|^2, \tag{30a}$$

$$R = \left|\frac{2\kappa_{\rm ex}}{\kappa}\frac{g_1 g_2}{|g_1|^2+|g_2|^2}\frac{2(C_{\rm tot}+C_{\rm tot}')}{1+2(C_{\rm tot}+C_{\rm tot}')}\right|^2, \tag{30b}$$

where $C_{\rm tot}' = (|g_1'|^2 + |g_2'|^2)/2\kappa(\gamma' + i\delta_a')$ is the complex cooperativity associated with the detuned second excited state. Not surprisingly, since the symmetry between the coupling strengths of both sides is maintained, the four-level system effectively behaves like a symmetric Λ system with cooperativity equal to the sum of the cooperativities of the separate transitions. However, if $s = -1$ we obtain

$$T = \left|\frac{2\kappa_{\rm ex}}{\kappa}\frac{|g_1|^2}{|g_1|^2+|g_2|^2}\frac{2(C_{\rm tot}+C_{\rm tot}')+16\frac{|g_1|^2+|g_2|^2}{|g_1|^2}C_1C_2'}{1+2(C_{\rm tot}+C_{\rm tot}')+16C_1C_2'} + t_0\right|^2, \tag{31a}$$

$$R = \left|\frac{2\kappa_{\rm ex}}{\kappa}\frac{g_1 g_2}{|g_1|^2+|g_2|^2}\frac{2(C_{\rm tot}-C_{\rm tot}')}{1+2(C_{\rm tot}+C_{\rm tot}')+16C_1C_2'}\right|^2, \tag{31b}$$

where we defined single-transition cooperativities $C_1 = |g_1|^2/2\kappa\gamma$ and $C_2' = |g_2'|^2/2\kappa(\gamma' + i\delta_a')$. In this case, the symmetry between the two "sides" of the system is broken, removing the balance necessary for SPRINT. Still, unit fidelity can be attained by slightly detuning the cavity. The necessary detuning and fiber-resonator coupling can be determined by replacing $\kappa_i \to \kappa_i + i\delta_C$ in Eq. (31a), and setting $T = 0$ for both the real and imaginary parts. A useful approximation is then obtained by taking $\gamma' \ll i\delta_a'$, reflecting the fact that the detuning of the second excited state is high compared to its linewidth. The optimal parameters then become

$$\delta_C^{\rm opt} = \kappa_i C_i'\frac{1+2C_i}{1+C_i}, \tag{32a}$$

$$\kappa_{\rm ex}^{\rm opt} = \kappa_i\sqrt{\left(1+2C_i'\frac{\gamma'}{\delta_a'} + \frac{C_i'^2}{(1+C_i)^2}\right)(1+2C_i)}, \tag{32b}$$

where we took $g_1 = g_2 \equiv g$, and $g_1' = -g_2' \equiv g'$ and defined the total intrinsic cooperativity of the detuned excited state $C_i' = |g'|^2/\kappa_i\delta_a'$.

IV. SIMULATIONS

A. Model

In this section we analyze the imperfections of SPRINT jointly and specific to its realization in Ref. [21], which uses ^{87}Rb atoms coupled to silica microsphere resonators. We already mentioned that the coupling constant between optical modes h should be taken into account. As for the nonideal polarization, calculation at the location where the atom feels the strongest field yields $r_\sigma \simeq 0.18$ for the opposite circular polarized field, and $r_\pi \simeq 0.13$ for the π-polarized field. The presence of the unwanted fields also entails that otherwise uncoupled atomic levels can now take part in the dynamics. In ^{87}Rb, all three ground states of $F = 1$ should then be taken into account [see Fig. 6(b)], as well as the excited state $F' = 0$ and all three excited states in $F' = 1$. Furthermore, another major hurdle is the fact that trapping atoms near WGM microresonators is a highly challenging task that has not yet been realized. As a result, the atoms fly past the microresonator or crash into its surface, causing the coupling strength to vary from run to run, and during a single run. This can be taken into account by assuming a normally distributed coupling strength with independently determined mean $\bar{g}$ and standard deviation σ_g, truncated at the minimally detectable and maximally available coupling strengths. Finally, the effect of different pulse lengths and shapes can be included by introducing a time-varying κ_s. All these effects can be taken into account

by simulating the evolution of the state of the system with the complete Hamiltonian, including all transitions of interest in ^{87}Rb:

$$\begin{aligned}\hat{H}_6 = {} & \hat{H}_4 + \hat{H}_{e'} - i(\gamma' + i\delta'_a)\hat{\sigma}_{e'_1e'_1} - i(\gamma' + i\delta'_a)\hat{\sigma}_{e'_2e'_2} \\ & - r_\sigma\left(g'^*\hat{a}^\dagger\hat{\sigma}_{2e'} + g'\hat{\sigma}^\dagger_{2e'}\hat{a}\right) + r_\sigma\left(g'\hat{b}^\dagger\hat{\sigma}_{1e'} + g'^*\hat{\sigma}^\dagger_{1e'}\hat{b}\right) \\ & - r_\pi\left(g'^*\hat{a}^\dagger\hat{\sigma}_{1e'_1} + g'\hat{\sigma}^\dagger_{1e'_1}\hat{a}\right) - r_\pi\left(g'\hat{b}^\dagger\hat{\sigma}_{1e'_1} + g'^*\hat{\sigma}^\dagger_{1e'_1}\hat{b}\right) \\ & + r_\pi\left(g'^*\hat{a}^\dagger\hat{\sigma}_{2e'_2} + g'\hat{\sigma}^\dagger_{2e'_2}\hat{a}\right) + r_\pi\left(g'\hat{b}^\dagger\hat{\sigma}_{2e'_2} + g'^*\hat{\sigma}^\dagger_{2e'_2}\hat{b}\right) \\ & + \left(g'^*\hat{a}^\dagger\hat{\sigma}_{0e'_2} + g'\hat{\sigma}^\dagger_{0e'_2}\hat{a}\right) - \left(g'\hat{b}^\dagger\hat{\sigma}_{0e'_1} + g'^*\hat{\sigma}^\dagger_{0e'_1}\hat{b}\right) \\ & - r_\sigma\left(g'^*\hat{a}^\dagger\hat{\sigma}_{0e'_1} + g'\hat{\sigma}^\dagger_{0e'_1}\hat{a}\right) + r_\sigma\left(g'\hat{b}^\dagger\hat{\sigma}_{0e'_2} + g'^*\hat{\sigma}^\dagger_{0e'_2}\hat{b}\right),\end{aligned} \tag{33}$$

where we used the fact that in our case all coupling strengths to a given excited state manifold are of equal magnitude. The signs, however, vary, and in particular, one should set $g'_1 = g'$ and $g'_2 = -g'$ in $\hat{H}_{e'}$, and $g_1 = g_2 = g$ in $\hat{H}_4$, resulting in the deterioration of SPRINT fidelity. The best strategy is to work with the $F = 1 \rightarrow F' = 1$ manifold on resonance, rather than with $F = 1 \rightarrow F' = 0$. This serves a double purpose: the efficiency of SPRINT can be increased, because $g' = \sqrt{5/4}g$, resulting in an increased cooperativity. For the same reason, the interference with the red-detuned $F = 1 \rightarrow F' = 0$ transitions is reduced.

In order to assess the performance of SPRINT in an actual experimental setting, we simulated the dynamics using realistic system parameters $(\kappa_i, \bar{g}, \sigma_g, h, \gamma, \gamma', \delta_a, \delta'_a) = 2\pi \times (6, 16, 6, 1, 3, 3, -72, 0)$ MHz [21]. Moreover, we used the optimal nanofiber-microresonator coupling rate and microresonator detuning $(\kappa_{ex}, \delta_C) = 2\pi \times (30, -7)$ MHz, a 53-ns full width at half maximum (FWHM) Gaussian input pulse, and a uniformly distributed atomic azimuthal location. As shown in Table I, a simulation using the Hamiltonian of Eq. (33) with the atom initialized in ground state G_1 results in an optimal SPRINT fidelity of ∼82%, and a photon loss probability of ∼51%. A reflection event heralds a successful transfer of the atom to the opposite ground state with a probability of ∼94%. After a first photon toggled the atom to G_2, a second photon that is sent from the source cavity still has some probability of being reflected, due to the nonideal circular polarization. A simulation with the atom initially in G_2 yields a normalized reflection probability of ∼3.5%, but this reflection no longer induces the Raman passage of the atom.

TABLE I. Statistics of atomic and photonic final states for (a) the atom initially in G_1, and (b), the atom initially in G_2. R stands for probability of reflection, T for probability of transmission, and L for probability of photon loss. The atom can either toggle to the other ground state, remain in the initial one, or end up in G_0 or in $F = 2$ [not shown in Fig. 6(b)], in which case it is considered lost.

(a)	R	T	L	Total
Toggle	39.97%	1.39%	17.03%	58.39%
No toggle	2.17%	4.18%	30.15%	36.50%
Atom lost	0.50%	0.43%	4.16%	5.09%
Total	42.64%	6.00%	51.34%	100%
(b)	R	T	L	Total
Toggle	0.06%	1.39%	0.59%	2.04%
No toggle	1.55%	41.97%	51.72%	95.24%
Atom lost	0.01%	1.76%	0.95%	2.75%
Total	1.62%	45.12%	53.26%	100%

We finally included the trajectory of the atoms falling on or around the microresonator. Because of surface effects, the dynamics of the atomic state is also taken into account [34,35]. Our calculations of the electric field in the evanescent region of a microsphere are based on [33]. Simulations with the above system parameters show that the resulting fidelity is about 75%.

B. Means to overcome SPRINT imperfections

This part numerically investigates to what extent the disruptions of the SPRINT mechanism induced by the parameters $(h, r_\sigma, r_\pi, \kappa_i)$ can be reduced by tuning two parameters accessible to the experimentalist, namely the nanofiber-microresonator coupling κ_{ex} and microresonator detuning δ_c, in order to retrieve a maximum SPRINT fidelity. The influence of each of these flaws is discussed separately. Unless otherwise specified, the numerical values of the system parameters are those of the previous section.

To begin with, we consider κ_{ex} as a means to improve the fidelity. We study first the behavior of the fidelity with respect to h, as shown in Fig. 7(a) for values of κ_{ex} ranging from 30 to $70\times2\pi$ MHz. Although the fidelity always drops with h, it can be efficiently optimized by varying κ_{ex}: for a value of $h = 2\pi\times20$ MHz, the fidelity increases by 36% when κ_{ex} is optimized. Specifically, the value of κ_{ex} needed to maximize the fidelity is shown in the inset, and the corresponding fidelity as the dashed line of the main frame. The analytical expressions of Eqs. (22) and (23) are a good approximation only for the restricted range $h \ll \kappa_i = 6\times2\pi$ MHz.

We study next the evolution of the fidelity with the nonideal polarization by considering r_σ, whose value exceeds that of r_π. Over the range $r_\sigma = [0,0.3]$ considered here, tuning κ_{ex} does not help to improve the fidelity, in conformity with the analytical results from Sec. III B 1. We therefore show in Fig. 7(b) the fidelity for $\kappa_{ex} = 30\times2\pi$ MHz. When these numerical simulations are performed in the framework of Sec. III B 1 (i.e., a three-level system driven by an exponentially decaying pulse, where r_σ is the only imperfection and g is constant), they are in perfect agreement with the analytical results of Eqs. 13 and 14.

In Fig. 7(c), we show the evolution of the fidelity with respect to the intrinsic loss parameter κ_i for various values of κ_{ex}. Accordingly, the optimal κ_{ex} and corresponding maximal fidelity are, respectively, presented in the inset and as a dashed line in the main frame. We see that the variation of the optimized fidelity within the range $\kappa_i = [0,20]\times2\pi$ MHz is as low as 3.5%, which shows the importance of choosing the appropriate κ_{ex}. Note, however, that a higher κ_i inevitably lowers the efficiency.

We turn next to the second parameter that one can access experimentally, the cavity detuning δ_C. Simulations show that tuning δ_C is beneficial only to restore the drop in fidelity arising from the presence of multiple excited states, resulting in a value of $\delta_C = -7\times2\pi$ MHz.

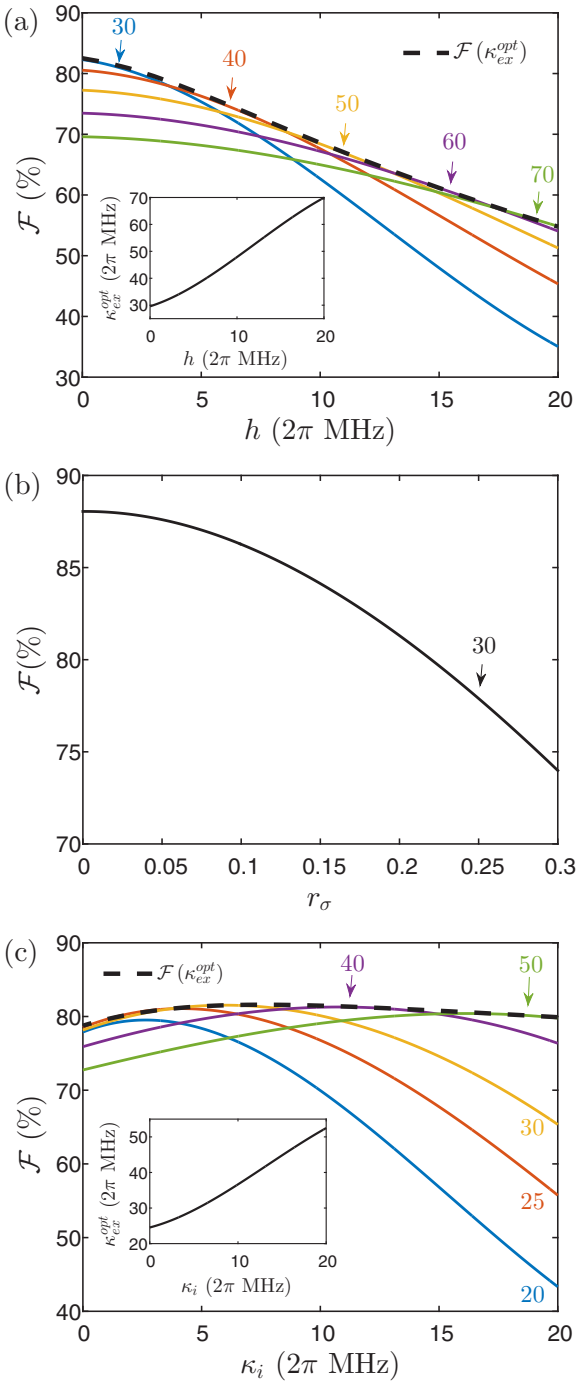

FIG. 7. Fidelity as a function of h (a), r_σ (b), and κ_i (c) for different values of κ_{ex} written in the figure in units of 2π MHz. For (a) and (c), the insets give the value of κ_{ex} that maximizes the fidelity; the corresponding maximal fidelity is shown as a dashed line in the main frames. In (b), $\mathcal{F}$ is insensitive to the choice of κ_{ex}.

Then, to sum up this part dedicated to the optimization of the fidelity regarding h, r_σ, r_π, and κ_i, we showed that κ_{ex} is the relevant parameter and can compensate for h and κ_i. The contour plots in Figs. 8(a) and 8(b) therefore give a direct reading of the optimal κ_{ex} (a) and the corresponding fidelity (b) for any h and κ_i within the range [0,20] MHz.

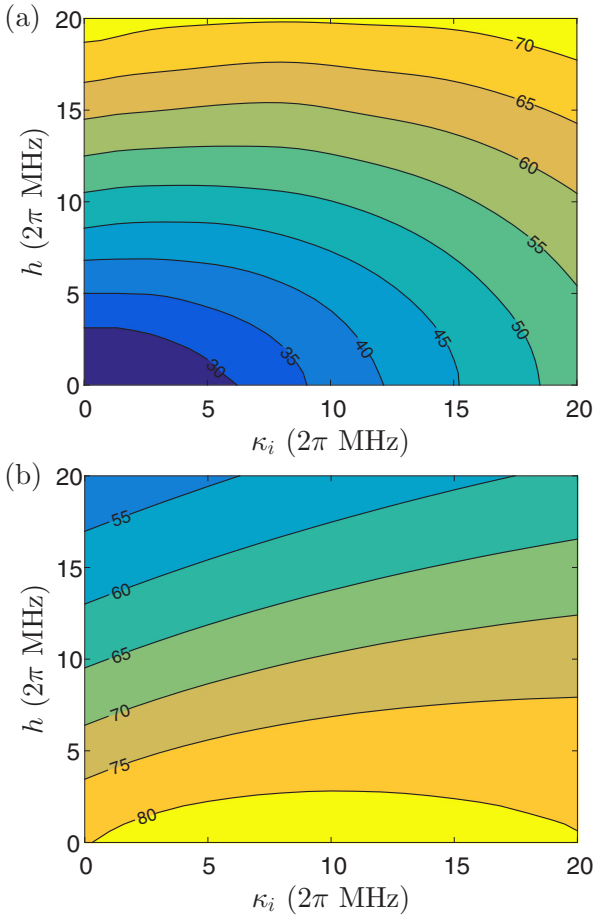

FIG. 8. Contour plots of (a) κ_{ex}^{opt} that maximizes the fidelity and (b) the corresponding maximal fidelity $\mathcal{F}(\kappa_{ex}^{opt})$ as a function of both h and κ_i.

We finish this section by noting that the application of a magnetic field so as to induce a Zeeman splitting of the energy levels would increase the fidelity for two reasons. First, it would reduce the r_σ and h coefficients, hence improve the directionality. Secondly, a spectral discrimination could be made on photons resulting from the atomic relaxation through the wrong transition.

C. Comparison to the analytical models

In this section, we compare the different analytical models of Sec. III with the previous numerical simulations. In order to do so, we present calculations and simulations that include separately or jointly the parameters h, r_σ, and r_π, the spread of the parameter g, and the actual energy levels of the ^{87}Rb D_2 line with multiple excited states. The resulting fidelity, optimized by κ_{ex} and δ_C, is shown in Fig. 9 as a function of κ_i. The solid lines correspond to the simulations involving a 53-ns FWHM Gaussian temporal input pulse in accordance with the experiment, while the dashed lines are the analytical calculations involving a long exponentially decaying input pulse. Unless otherwise specified below, the parameters are those from Sec. IV A.

The plot (1) corresponds to the model of Sec. III A where only the Λ system $F = 1 \rightarrow F' = 1$ is involved, the

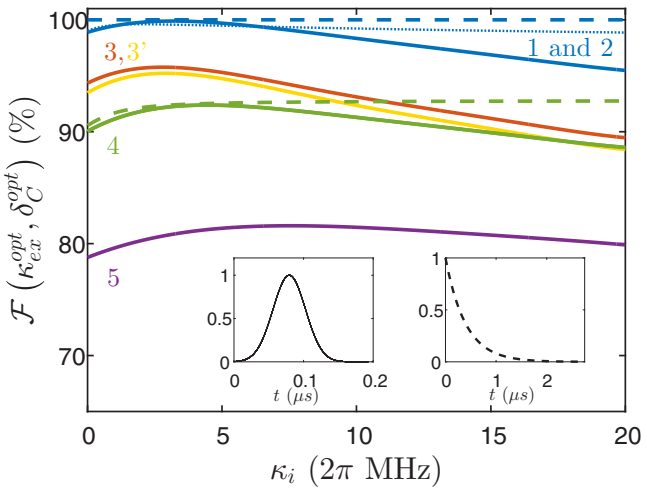

FIG. 9. Simulations of the fidelity maximized by tuning κ_{ex} and δ_C, as a function of κ_i. In solid lines, simulations with a realistic Gaussian input pulse (left inset) taking into account the transient dynamics. In dashed lines, calculations only involving the steady state with a long input pulse (here exponentially decaying, right inset); simulations with a wide Gaussian pulse coincide. Labels 1–5 refer to the following:

	1	2	3, 3'	4	5
Λ-system $F \to F'$	$1 \to 1$	$\mathbf{1 \to 1}$ **and** $\mathbf{1 \to 0}$	(3) $1 \to 1$ (3') $1 \to 0$	$1 \to 1$	actual level scheme
g	$\bar{g}$	$\bar{g}$	**gaussian spread**	$\bar{g}$	gaussian spread
h, r_σ, r_π	0	0	0	$\mathbf{\neq 0}$	$\neq 0$
model from Sec.	III A	III E		III D	IV A

The dashed line 1 becomes the dotted line 1 when the transient dynamics is considered, with $\kappa_s = 0.1 \times 2\pi$ MHz. In all cases, $\gamma = 3 \times 2\pi$ MHz.

g parameter is taken constant ($g = \bar{g}$), and $h = r_\sigma = r_\pi = 0$. One setting at a time is then changed in (2), (3), and (4). Specifically, (2) involves two excited states as in Sec. III E [see Fig. 6(a)]. We note that its optimized fidelity coincides with that of (1). (3) takes into account the spread of g. It is presented in two variants depending on which Λ system is chosen, and only a small difference occurs. (4) sets $h \neq 0$, $r_\sigma \neq 0$, and $r_\pi \neq 0$ as in Sec. III D. Finally, (5) is the full realistic simulation already shown in Fig. 7(c) that takes into account all the previous sources of loss jointly.

First of all, a discrepancy occurs between the two sets of curves, in solid and dashed lines. It arises from the transient temporal dynamics, which was not included in the analytical models of the previous sections. In particular, we see that the solid curve (1) does not reach unity for all κ_i, not even for $\kappa_i = 0$ MHz because of nonzero γ, unlike the dashed curve (1) that is always at steady state. Still, the fidelity is only affected by a few percents, which shows the validity of our analytical approach. Both sets of curves coincide for long enough Gaussian input pulses, of the order of 1 μs FWHM. A further comparison to the analytical models is given from a derivation that includes the transient dynamics in the case of ideal SPRINT with exponentially decaying input pulse. It is presented in Appendix A and results in the dotted line 1 presented in Fig. 9 for $\kappa_s = 0.1 \times 2\pi$ MHz. The fidelity tends to reach one when κ_s decreases.

Next, we see that the deterioration of the optimized fidelity is primarily due to nonzero h, r_σ, and r_π (7.8%, at our experimental value $\kappa_i = 2\pi \times 6$ MHz), then to the spread of g (5.1%), and to a very small extent to the transient temporal dynamics (0.5%). The presence of a second excited state that enables an extra pathway for SPRINT does not affect the fidelity by virtue of tuning κ_{ex} and δ_C.

V. CONCLUSION

In this work we analyzed the performance of single-photon Raman interaction, which operates as a SWAP gate between an optical and a material qubits. SPRINT is inherently deterministic and passive since no active control of the material state is required. As such it is also orders of magnitude faster than active protocols, since it occurs on the time scale of the cavity-enhanced spontaneous emission rate (a few ns). We defined the process fidelity $\mathcal{F}$, which provides a lower limit for the SWAP gate fidelity. We showed its robustness against various experimental flaws. While atomic emission to free space and intrinsic cavity losses unavoidably result in photon loss (reduced efficiency), the fidelity can still be optimized by choosing the coupling rate between the nanofiber and the microresonator appropriately, even in the case of parasitic coupling between the optical modes, albeit at the price of further lowering the efficiency. The effect of multiple excited states that disrupts the operation of SPRINT can be annulled by slightly detuning the cavity resonance. The analysis presented in this work provides the tools for realistic optimization of SPRINT, applicable to any three-level Λ system, bringing it into the regime in which it could form the basis for a scalable quantum network.

ACKNOWLEDGMENTS

This work was partially supported by the Israel Science Foundation, the Wolfson Foundation, and the Crown Photonics Center. This research was made possible in part by the historic generosity of the Harold Perlman Family.

S.R. and A.B. contributed equally to this work.

APPENDIX: IDEAL SPRINT WITH TRANSIENT TEMPORAL DYNAMICS

This appendix gives an analytical resolution of the ideal SPRINT governed by the Hamiltonian $\hat{H}_0$ from Eq. (2) in the case where the state $|\psi(t)\rangle$ from Eq. (3) cannot be considered to be at steady state at all times. The evolution of its probability amplitudes is given by

$$\begin{aligned}\alpha(t) &= -c_1 e^{-\kappa t} + g_1^*[c_- v_+ e^{-\lambda_+ t} + c_+ v_- e^{-\lambda_- t}] + \alpha_0,\\ \beta(t) &= c_1 e^{-\kappa t} + g_2[c_- v_+ e^{-\lambda_+ t} + c_+ v_- e^{-\lambda_- t}] + \beta_0, \quad \text{(A1)}\\ \xi(t) &= c_- e^{-\lambda_+ t} + c_+ e^{-\lambda_- t} + \xi_0,\end{aligned}$$

where

$$\lambda_\pm = \frac{1}{2}(\gamma+\kappa \pm \sqrt{(\gamma-\kappa)^2 - 4(|g_1|^2+|g_2|^2)}), \quad v_\pm = \frac{2i}{\gamma-\kappa \pm \sqrt{(\gamma-\kappa)^2 - 4(|g_1|^2+|g_2|^2)}},$$
$$c_1 = -2\frac{\sqrt{\kappa_s\kappa_{ex}}}{\kappa-\kappa_s}\frac{g_1 g_2}{|g_1|^2+|g_2|^2}e^{-\kappa_s t}, \quad c_\pm = \pm\frac{2\sqrt{\kappa_s\kappa_{ex}}}{v_- - v_+}\frac{g_1}{|g_1|^2+|g_2|^2}\frac{1}{1+2C_{\rm tot}}e^{-\kappa_s t}\left(\frac{1}{\kappa-\kappa_s}+2iC_{\rm tot}v_\pm\right), \tag{A2}$$

and α_0, β_0, and ξ_0 are α, β and ξ from Eq. (5) with

$$C_{\rm tot} = \frac{|g_1|^2+|g_2|^2}{2(\kappa-\kappa_s)(\gamma-\kappa_s)}. \tag{A3}$$

[1] H. J. Kimble, Nature (London) **453**, 1023 (2008).
[2] N. H. Nickerson, Y. Li, and S. C. Benjamin, Nat. Commun. **4**, 1756 (2013).
[3] N. H. Nickerson, J. F. Fitzsimons, and S. C. Benjamin, Phys. Rev. X **4**, 041041 (2014).
[4] S. Haroche and J. M. Raimond, *Exploring the Quantum: Atoms, Cavities, and Photons (Oxford Graduate Texts)* (Oxford University Press, New York, 2013).
[5] R. J. Thompson, G. Rempe, and H. J. Kimble, Phys. Rev. Lett. **68**, 1132 (1992).
[6] L.-M. Duan and H. J. Kimble, Phys. Rev. Lett. **92**, 127902 (2004).
[7] A. Reiserer, S. Ritter, and G. Rempe, Science **342**, 1349 (2013).
[8] T. G. Tiecke, J. D. Thompson, N. P. de Leon, L. R. Liu, V. Vuletić, and M. D. Lukin, Nature (London) **508**, 241 (2014).
[9] A. Reiserer, N. Kalb, G. Rempe, and S. Ritter, Nature (London) **508**, 237 (2014).
[10] N. Kalb, A. Reiserer, S. Ritter, and G. Rempe, Phys. Rev. Lett. **114**, 220501 (2015).
[11] B. Hacker, S. Welte, G. Rempe, and S. Ritter, Nature (London) **536**, 193 (2016).
[12] D. Pinotsi and A. Imamoglu, Phys. Rev. Lett. **100**, 093603 (2008).
[13] G. Lin, X. Zou, X. Lin, and G. Guo, Europhys. Lett. **86**, 30006 (2009).
[14] K. Koshino, S. Ishizaka, and Y. Nakamura, Phys. Rev. A **82**, 010301 (2010).
[15] J. Gea-Banacloche and L. M. Pedrotti, Phys. Rev. A **83**, 042333 (2011).
[16] J. Gea-Banacloche and L. M. Pedrotti, Phys. Rev. A **86**, 052311 (2012).
[17] S. Rosenblum, S. Parkins, and B. Dayan, Phys. Rev. A **84**, 033854 (2011).
[18] J. Gea-Banacloche and W. Wilson, Phys. Rev. A **88**, 033832 (2013).
[19] M. Bradford and J.-T. Shen, Phys. Rev. A **85**, 043814 (2012).
[20] M. Bradford, K. C. Obi, and J.-T. Shen, Phys. Rev. Lett. **108**, 103902 (2012).
[21] I. Shomroni, S. Rosenblum, Y. Lovsky, O. Bechler, G. Guendelman, and B. Dayan, Science **345**, 903 (2014).
[22] S. Rosenblum, O. Bechler, I. Shomroni, Y. Lovsky, G. Guendelman, and B. Dayan, Nat. Photon. **10**, 19 (2016).
[23] K. Inomata, K. Koshino, Z. R. Lin, W. D. Oliver, J. S. Tsai, Y. Nakamura, and T. Yamamoto, Phys. Rev. Lett. **113**, 063604 (2014).
[24] K. Inomata, Z. Lin, K. Koshino, W. D. Oliver, J.-S. Tsai, T. Yamamoto, and Y. Nakamura, Nat. Commun. **7**, 12303 (2016).
[25] If the two-level system is coupled to just one direction of the waveguide, the radiated field is twice as strong, resulting in a π phase shift of the transmitted probe, instead of destructive interference. The saturation of this effect at the single-photon level results in a nonlinear phase shift [8,36].
[26] D. K. Armani, T. J. Kippenberg, S. M. Spillane, and K. J. Vahala, Nature (London) **421**, 925 (2003).
[27] C. Junge, D. O'Shea, J. Volz, and A. Rauschenbeutel, Phys. Rev. Lett. **110**, 213604 (2013).
[28] J. Petersen, J. Volz, and A. Rauschenbeutel, Science **346**, 67 (2014).
[29] P. Lodahl, S. Mahmoodian, S. Stobbe, A. Rauschenbeutel, P. Schneeweiss, J. Volz, H. Pichler, and P. Zoller, Nature **541**, 473 (2017).
[30] H. J. Carmichael, Phys. Rev. Lett. **70**, 2273 (1993).
[31] C. W. Gardiner and M. J. Collett, Phys. Rev. A **31**, 3761 (1985).
[32] For example, this condition can be automatically satisfied in ^{87}Rb by using the three-level Zeeman manifold of either the $F=1$ to $F'=0$ transition (as in Ref. [21]) or the $F=1$ to $F'=1$ transition.
[33] B. Johnson, J. Opt. Soc. Am. A **10**, 343 (1993).
[34] S.-T. Wu and C. Eberlein, in *Proceedings of the Royal Society of London A: Mathematical, Physical and Engineering Sciences* (The Royal Society, London, 1999), Vol. 455, p. 2487.
[35] M. S. Safronova, C. J. Williams, and C. W. Clark, Phys. Rev. A **69**, 022509 (2004).
[36] J. Volz, M. Scheucher, C. Junge, and A. Rauschenbeutel, Nat. Photon. **8**, 965 (2014).